

Figs. 3 and 4 show Pt species located randomly on the ceria surfaces (not embedded in the ceria), with no preference for specific facets.

Atom trapping should be broadly applicable as a method for preparing single-atom catalysts. The approach requires a supply of mobile atoms and a support that can bind the mobile species. Conditions that are conducive to Ostwald ripening, which normally is implicated in the degradation of catalysts (3), are ideal because mobile species are continually being generated. In our work, at the aging temperature of 800°C in air, mobile PtO₂ is rapidly emitted; the estimated lifetime is only a few seconds for a 5-nm Pt crystallite (24). Surface species such as hydroxyls and carbonates, which could prevent the trapping of mobile species, would have desorbed at high temperatures, providing a clean surface for the formation of covalent metal oxide bonds that are needed to stabilize single atoms. Trapping of atoms provides a plausible explanation for the role of ceria in slowing the rates of Ostwald ripening and may help to explain how other supports modify the rates of catalyst sintering.

REFERENCES AND NOTES

- G. W. Graham *et al.*, *Catal. Lett.* **116**, 1–8 (2007).
- M. H. Wiebenga *et al.*, *Catal. Today* **184**, 197–204 (2012).
- T. W. Hansen, A. T. Delariva, S. R. Challa, A. K. Datye, *Acc. Chem. Res.* **46**, 1720–1730 (2013).
- T. R. Johns *et al.*, *J. Catal.* **328**, 151–164 (2015).
- J. A. Kurzman, L. M. Misch, R. Seshadri, *Dalton Trans.* **42**, 14653–14667 (2013).
- C. B. Alcock, G. W. Hooper, *Proc. R. Soc. London Ser. A* **254**, 551–561 (1960).
- G. Cavataio *et al.*, *SAE Int. J. Fuels Lubr.* **2**, 204–216 (2009).
- Y.-F. Yu-Yao, J. T. Kummer, *J. Catal.* **106**, 307–312 (1987).
- J. G. McCarty, K.-H. Lau, D. L. Hildenbrand, *Stud. Surf. Sci. Catal.* **111**, 601–607 (1997).
- C. Carrillo *et al.*, *J. Phys. Chem. Lett.* **5**, 2089–2093 (2014).
- G. B. McVicker, R. L. Garten, R. T. K. Baker, *J. Catal.* **54**, 129–142 (1978).
- Y. Nagai *et al.*, *J. Catal.* **242**, 103–109 (2006).
- J. A. Farmer, C. T. Campbell, *Science* **329**, 933–936 (2010).
- J. H. Kwak *et al.*, *Science* **325**, 1670–1673 (2009).
- B. Qiao *et al.*, *Nat. Chem.* **3**, 634–641 (2011).
- W.-Z. Li *et al.*, *Nat. Commun.* **4**, 2481 (2013).
- T. R. Johns *et al.*, *ChemCatChem* **5**, 2636–2645 (2013).
- H.-X. Mai *et al.*, *J. Phys. Chem. B* **109**, 24380–24385 (2005).
- S. Agarwal *et al.*, *ChemSusChem* **6**, 1898–1906 (2013).
- T. Wu *et al.*, *J. Phys. Chem. Lett.* **5**, 2479–2483 (2014).
- A. Bruix *et al.*, *Angew. Chem. Int. Ed.* **53**, 10525–10530 (2014).
- A. Neitzel *et al.*, *J. Phys. Chem. C* **120**, 9852–9862 (2016).
- Z. L. Wang, X. Feng, *J. Phys. Chem. B* **107**, 13563–13566 (2003).
- See supplementary materials on Science Online.
- P. J. Berlowitz, C. H. F. Peden, D. W. Goodman, *J. Phys. Chem.* **92**, 5213–5221 (1988).
- R. Kopelelt *et al.*, *Angew. Chem. Int. Ed.* **54**, 8728–8731 (2015).
- M. Cargnello *et al.*, *Science* **341**, 771–773 (2013).
- M. Moses-DeBusk *et al.*, *J. Am. Chem. Soc.* **135**, 12634–12645 (2013).
- K. Ding *et al.*, *Science* **350**, 189–192 (2015).
- F. Dvořák *et al.*, *Nat. Commun.* **7**, 10801 (2016).

ACKNOWLEDGMENTS

Supported by NSF GOALI grant CBET-1438765 (J.J., H.X., S.R.C., A.K.D.), General Motors Global R&D (G.Q., S.O., and M.H.W.), U.S. Department of Energy grant DE-FG02-05ER15712 (A.T.D., E.J.P., A.K.D., X.L.P.H., and Y.W.), and the Center for Biorenewable Chemicals funded by NSF grant EEC-0813570 (H.X., H.P., and A.K.D.). This work made use of the JEOL JEM-ARM200CF at the University of Illinois at Chicago. We thank A. Nicholls for

recording the AC-STEM images and D. Kunwar for assistance in catalyst preparation.

SUPPLEMENTARY MATERIALS

www.sciencemag.org/content/353/6295/150/suppl/DC1
Materials and Methods

Figs. S1 to S14
Tables S1 to S3
References (31–35)

26 April 2016; accepted 13 June 2016
10.1126/science.aaf8800

ANIMAL ROBOTICS

Tail use improves performance on soft substrates in models of early vertebrate land locomotors

Benjamin McInroe,^{1*} Henry C. Astley,^{1*} Chaohui Gong,² Sandy M. Kawano,³ Perrin E. Schiebel,¹ Jennifer M. Rieser,¹ Howie Choset,² Richard W. Blob,⁴ Daniel I. Goldman^{1,5,†}

In the evolutionary transition from an aquatic to a terrestrial environment, early tetrapods faced the challenges of terrestrial locomotion on flowable substrates, such as sand and mud of variable stiffness and incline. The morphology and range of motion of appendages can be revealed in fossils; however, biological and robophysical studies of modern taxa have shown that movement on such substrates can be sensitive to small changes in appendage use. Using a biological model (the mudskipper), a physical robot model, granular drag measurements, and theoretical tools from geometric mechanics, we demonstrate how tail use can improve robustness to variable limb use and substrate conditions. We hypothesize that properly coordinated tail movements could have provided a substantial benefit for the earliest vertebrates to move on land.

During the vertebrate invasion of land, 385 to 360 million years ago, early tetrapods and relatives faced a variety of challenges (1), including locomotion in terrestrial environments. Terrestrial locomotion relies on interactions between the body and substrate to generate propulsive forces, but the interaction between the organism and some substrates may be complex. Fossil evidence indicates that tetrapods emerged from water in near-shore habitats, where they likely encountered flowable soft substrates such as sands and muds (2, 3). These substrates exhibit properties of solids and fluids, either jamming or yielding (plastic deformation of the material) depending on how they are loaded (4) and sloped (5).

The challenge of movement on flowable substrates therefore arises from the complexity of interactions between the substrate and the organism. Even on level deformable substrates, subtle variations in limb morphology (6) and kinematics (7) can lead to substantial differences in performance. Furthermore, interactions between appendages and these substrates leave

local disturbances, which can influence subsequent interactions, sometimes leading to deteriorating locomotor performance and eventual total locomotor failure (8). As substrate slope increases, yield forces decrease and downhill material flow becomes important, reducing the range of effective locomotor strategies (5).

The use of an additional locomotor structure that can be independently coordinated may allow a greater range of effective behaviors, even in the absence of derived limb morphology and sophisticated motor patterns. We propose that the tail could have been a critical locomotor structure for early tetrapods. In addition to being a primary driver of aquatic locomotion, tails play major roles in the propulsion of many modern fishes during terrestrial locomotion (9–12) and can be used as inertial reorientation appendages in some tetrapods (13, 14). Thus, the use of a prominent tail [as seen in fossil taxa (15–17) (Fig. 1A)] may have increased locomotor robustness to environmental and kinematic variables.

Evaluating locomotor performance for extinct taxa is challenging (18, 19), in part because the sensitivity of locomotion on complex substrates to kinematics and control strategies cannot necessarily be inferred from range of motion and morphology (7). Therefore, to test our hypothesis, we used three complementary modeling methods (Fig. 1): a model organism, a robophysical model, and a mathematical model. We made several choices governing our modeling approaches. In our locomotors, we modeled symmetrical, forelimb-driven

¹School of Physics, Georgia Institute of Technology, Atlanta, GA, USA. ²Robotics Institute, Carnegie Mellon University, Pittsburgh, PA, USA. ³National Institute for Mathematical and Biological Synthesis, University of Tennessee, Knoxville, TN, USA. ⁴Department of Biological Sciences, Clemson University, Clemson, SC, USA. ⁵School of Biology, Georgia Institute of Technology, Atlanta, GA, USA.

*These authors contributed equally to this work. †Corresponding author. Email: daniel.goldman@physics.gatech.edu

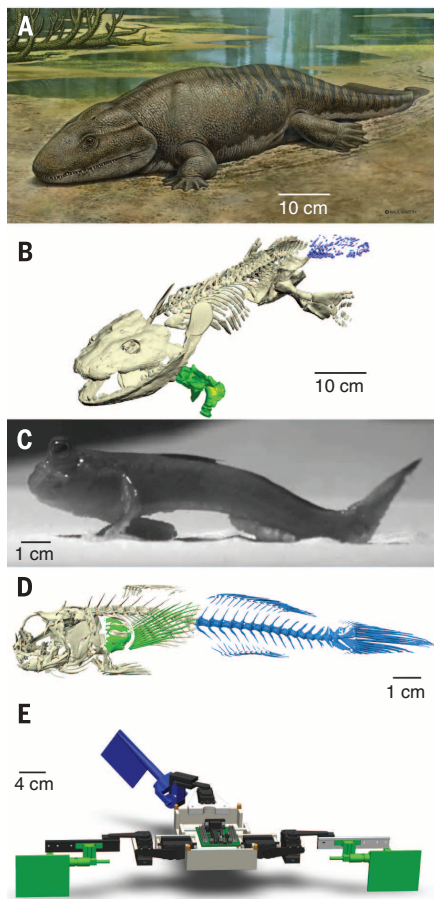


Fig. 1. Target and model systems for understanding early tetrapod locomotion on granular media.

(A) A reconstruction of *Ichthyostega* (~360 million years ago), an example of an early tetrapod body plan, by Raul Martin. (B) Skeletal reconstruction of *Ichthyostega*, an example of an early tetrapod body plan [from (20)], highlighting the pectoral limbs (green) and tail (blue). (C) The mudskipper (*Periophthalmus barbarus*), a biological model for early terrestrial locomotors. (D) A micro-computed tomography scan reconstruction of a mudskipper skeleton, highlighting the pectoral fin (green) and tail (blue). (E) The MuddyBot, a 3D printed robot developed to model the locomotion of crutching early tetrapods. Limbs are in green and the tail is in blue.

crutching locomotion (rather than salamander-like movement) in accordance with recent studies of *Ichthyostega* (20, 21); this choice enabled simplicity of control (coordinating two appendages rather than four) and obviated the need for continuous, stable support of an elevated body. We note that we are not strictly modeling *Ichthyostega*, nor any specific fossil taxon associated with the water-land transition, but are instead seeking general principles underlying limbed, crutching locomotion on yielding media.

Our biological model is the mudskipper (*Periophthalmus barbarus*) (12, 18, 20–24), a small fish that frequently moves terrestrially using synchronous motions of the pectoral fins, although these animals can use their tails for rapid jumping

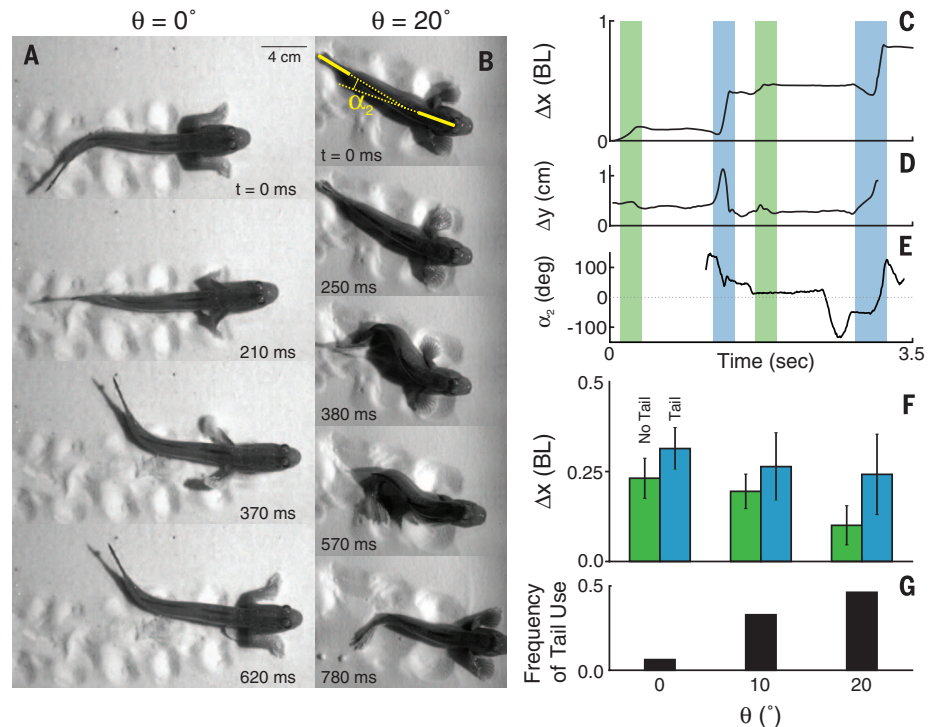


Fig. 2. Mudskipper locomotion on granular media at different substrate inclines (θ). (A and B) Dorsal-view video frames of a mudskipper fish on dry, loose sand inclined at 0° (A) and 20° (B) (movies S1 and S2). Yellow solid lines along the longest tail fin ray and from between the eyes to the anterior edge of the dorsal fin are used to compute the tail angle (α_2) in (E). The tail is not used propulsively in (A), although it moves slightly; in (B), the tail is used for propulsion. (C to E) Horizontal forward displacement per cycle (Δx) in body lengths (BL) for a single trial (C), vertical displacement (Δy , measured from eye) (D), and tail angle (α_2) (E) of mudskippers on sand at 20° incline. Cycles without tail use are indicated by green regions; cycles with tail use are indicated by blue regions (determined from video inspection). Missing values of α_2 are when the tail fin was out of view. (F) Δx at all inclines (θ) for steps without (green) and with (blue) tail use. Error bars denote SD. (G) Percentage of cycles with propulsive tail use across substrate inclines.

despite unspecialized tail morphology (25). Our robophysical model (Fig. 1E) (26) was designed with morphology representing the simplest possible version of a crutching locomotor, allowing us to systematically explore performance over a range of locomotor movements, including those movements not used by our biological model. Our mathematical model relies on the framework of geometric mechanics (27, 28) and allows us to understand how certain aspects of performance relate to coordination of limbs and tail. Our use of dry granular media was another modeling choice: The first vertebrates to move on land likely did so in wet shoreline habitats (such as mudflats) with properties that differ from those of dry granular media, but these media are united in displaying plastic deformation once the yield stress is exceeded (29–31). Although partially wet soils can display cohesion that increases yield stresses and results in larger “memory” effects, these rheological similarities [combined with the difficulty of preparing large volumes of standardized wet granular media (30)] led us to use dry media to model flowable substrates in our trials (30, 31).

Mudskippers ($N = 6$) were capable of effective locomotion over a level ($\theta = 0^\circ$) granular substrate [loose-packed dry oolite sand (table S1)]

using a crutching gait actuated by synchronous retraction of the pectoral fins with the tail angle (α_2) almost straight ($21^\circ \pm 22^\circ$; all measurements are means \pm SD) (Fig. 2A and movie S1), moving an average forward distance per cycle (Δx) of 0.21 ± 0.03 body lengths (BL) (Fig. 2F). During locomotion, mudskippers were able to fold the fin rays of the caudal and anal fins away from the substrate, allowing terrestrial locomotion without damage to or interference from these structures (Fig. 2B).

In some locomotor cycles, mudskippers used their tails (Fig. 2B and movie S2), bending the tail and planting the distal end of the tail and fin rays in the sand approximately orthogonal to the body axis ($119^\circ \pm 21^\circ$) (Fig. 2E) before retracting the pectoral fins and straightening the tail during the propulsive phase (Fig. 2B). Tracks left by these trials typically consisted of a series of paired impressions from the pectoral fins (sometimes obscured by yielding flow from subsequent steps, especially on inclines), with tail use leaving an additional impression offset to the right or left and overlapping the previous fin impressions (Fig. 2, A and B, and movies S1 and S2). Steps using the tail resulted in a higher displacement of 0.28 ± 0.08 BL on horizontal media (Fig. 2, C, D, and F).

As substrate incline angle increased, crutching with only the pectoral fins became less effective (Fig. 2F) and the frequency of steps for which the tail was used propulsively increased, from 6% on level substrate to 36% on substrate inclined at 10° and to 55% on substrate inclined at 20° (Fig. 2G). In addition to increasing displacement per cycle, tail use prevented downhill slip on inclined media when the tail was planted. The disparity in forward displacement increased between steps with and without tail use as substrate angle increased (Fig. 2F). At a 10° incline, mudskippers moved forward an average of 0.16 ± 0.03 BL with each step, versus 0.18 ± 0.08 BL when the tail was used (Fig. 2F). When the substrate was inclined to 20° , displacement was 0.07 ± 0.03 BL without tail use, increasing to 0.14 ± 0.07 BL with tail use (Fig. 2F). Further, mudskippers would occasionally jump clear of the test arena via tail-powered movements, indicating that the use of tails during crutching locomotion is controlled and submaximal.

A robophysical model of a crutching locomotor with limbs (Fig. 3A) allowed systematic testing of how locomotor performance in realistic granular environments was affected by variations in foot placement, limb adduction, and tail use (7). We elected to use a highly simplified morphology (a pair of laterally positioned, synchronously moving forelimbs and a posterior tail) (Fig. 3A) in order to focus on overarching locomotor control principles (“templates”) as opposed to the details of their anatomical implementation (“anchors”) (32). Although this model is simplified, it possesses some of the degrees of freedom seen in the mudskippers, namely the ability to control both body lifting (via limb adduction) and the interface with the substrate (limb supination) as well as use of the tail.

In addition to varying the incline ($\theta = 0^\circ$, 10° , and 20°) of the granular material, we varied three parameters of the robot: limb adduction angle (ψ), limb supination angle (ϕ), and presence or absence of tail use (Fig. 3). Adduction angle and the resultant lifting of the body is known to affect locomotor performance in similar robots on granular media (8) and may have been critical to terrestrial locomotion in early tetrapods (20). Supination angle, a simplified model of differences in limb placement, varied from a vertical limb insertion into the media (0°) to nearly flat (60°) in 15° increments. The tail was either used or not used, resulting in the posterior portion of the robot dragging in the media. In all cases, tail use induced alternating lateral rotations and displacements; although these yaw movements were often small ($<10^\circ$), they explain the few instances in which tail use was detrimental. To prevent damage to the motors, instead of sand we used two granular materials, loosely packed poppy seeds and spherical plastic particles (table S1) (33); prior work has shown that these substrates function well as models of more natural granular media (8, 33). Although the robot’s movements were slower than those of the mudskippers, all three substrates showed no dependence of force on speed over the ranges observed (~ 5 to 10 cm/s) (fig. S6).

In each trial, the robot performed a total of six limb cycles, the maximum number possible for the size of the bed. Insufficient first-step displacement has been shown to produce interactions with the previously disturbed media, resulting in lower displacement and further interactions until complete failure (stranding) (8). Conversely, if the first step is sufficient to prevent this interaction, the likelihood of failure decreases. In our experiments, few configurations produced intermediate displacements that led to decaying performance; most were either consistently successful or immediate failures (fig. S1). These trials were not sufficiently numerous to determine whether tail use altered the rate of decay, although it may do so indirectly if it increases first-step displacement. Consequently, we present data for only the first step (Δx_1).

To characterize how the adduction, supination, and tail use parameters affected the robot’s locomotion in undisturbed media, we measured Δx_1 for three trials per configuration (Fig. 3, D and E). During these trials, high values of adduction (which resulted in lifting much of the body clear of the substrate) and use of the tail improved first-step displacement, although not in a simple, addi-

tive manner; supination angle had an additional, minor influence (Fig. 3, D and E). On the level substrate, increasing adduction angle led to the largest performance increase, with supination angles of 30° and tail use resulting in modest improvements at lower adduction angles but offering minimal improvement over performance at the highest adduction angle (Fig. 3, B and D). At higher substrate angles with consequently lower granular yield forces, the role of the tail became dominant; effective locomotion without the tail was possible only at the highest adduction and lowest supination angles, but the use of the tail allowed locomotion over a wide range of limb kinematics (Fig. 3, C and E). In many of these cases, the use of the tail was the difference between success and failure [at $\theta = 20^\circ$, there were 15 failures among the 30 different configurations of ϕ and ψ (Fig. 3, D and E)]. Thus, the tail was not simply a uniform addition of propulsive force conferring a uniform advantage, as it did little to improve performance under near-optimal conditions. Instead, the tail had the greatest benefit when locomotion was otherwise compromised or ineffective as a result of low adduction angle or high substrate angle. A second set of trials

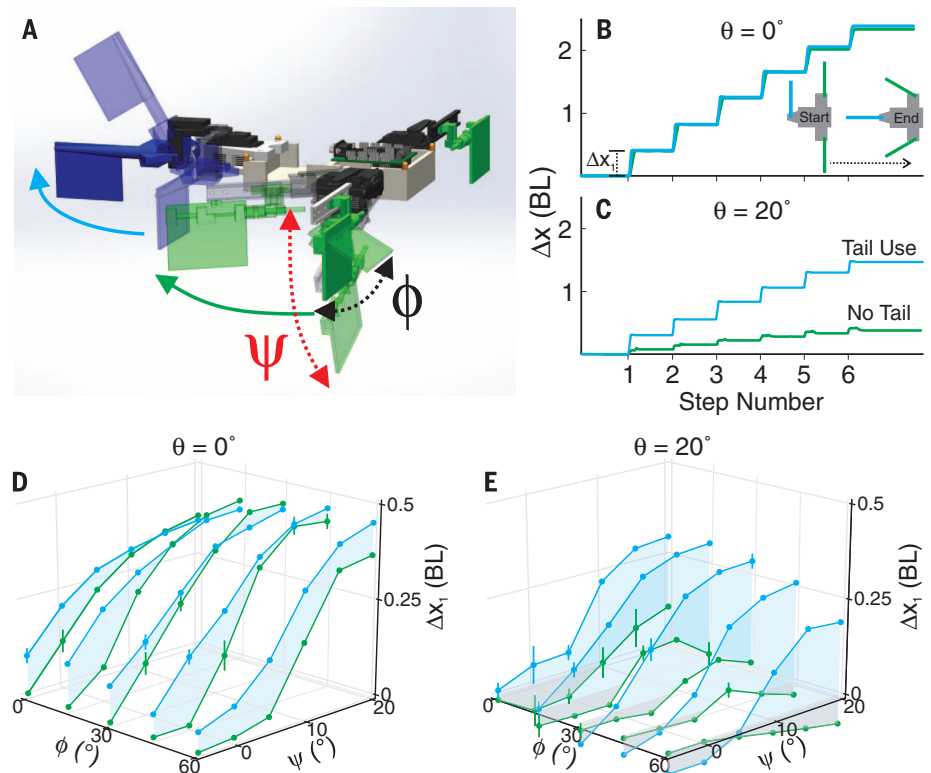


Fig. 3. Robophysical experiments on granular media at various substrate inclines (θ). (A) 3D model of MuddyBot, showing ranges of motion for limb retraction (green arrow, 60°) and tail motion (blue arrow, 90°). Limb adduction (ψ , -5° to 20° , where 0° is horizontal) and limb supination (ϕ , 0° to 60° , where 0° is vertical to the limb) are labeled, with other arrows showing directions of limb and tail motion during thrust phase. (B and C) Kinematics of a single trial of MuddyBot ($\phi = 15^\circ$, $\psi = 15^\circ$) moving for six cycles, without tail use (green) and with tail use (blue), on level ($\theta = 0^\circ$) (B) and inclined ($\theta = 20^\circ$) (C) poppy seeds. (D and E) First-step net displacement versus adduction and supination angles on $\theta = 0^\circ$ (D) and $\theta = 20^\circ$ (E) poppy seeds. Blue shading shows regions of identical supination angle for clarity. Vertical lines denote SD > 0.01 . Gray shading indicates negative values.

conducted using a different granular material showed qualitatively similar results [spherical plastic particles (table S1)], indicating that these results are robust to different granular media of different particle size and friction (figs. S2 and S5).

To gain insight into effective coordination of locomotor structures, we created a mathematical planar model of the robot using geometric

mechanics. This method, developed as a theoretical framework to elucidate principles of movement (27), describes how the self-deformation of the body (in our case, limb or tail movements) (Fig. 4A) generates net translation (or rotation) of the body. Geometric mechanics has been useful for understanding robot swimming (cyclic self-deformation due to traveling-wave body undulation) within granular media in which

inertial forces were small relative to frictional forces (28).

The geometric mechanics framework relies on construction of a “local connection” (34), which can be visualized as vector fields representing the link between small self-deformations (changes in the locomotor’s shape space, the set of internal shapes the mechanism can assume, here defined by planar limb and tail angles; Fig. 4A) and the resulting movement in world space (Fig. 4, D and E). For any given body configuration (a point in the diagrams in Fig. 4, D and E), the corresponding vector indicates the body deformation pattern that results in maximal forward movement. That is, if the robot begins from an arbitrary limb and tail angle combination (Fig. 4A), which corresponds to a horizontal and vertical location on the vector field (Fig. 4, D and E), a self-deformation parallel to the vector at that location will produce the greatest world-space incremental displacement, whereas self-deformations perpendicular to that vector will produce zero displacement. The overall pattern of a vector field allows visualization of how a time-varying pattern of self-deformations—represented as a path in the shape space—results in translation (or rotation). The net movement for a given sequence of limb and tail movements can be evaluated via a line integral in the vector field, with more effective motor patterns represented as paths that locally align more closely with vectors and pass through vectors of larger magnitudes (Fig. 4, D and E) (24).

Construction of local connection vector fields requires knowledge of how limb and tail segments experience drag forces. Because fundamental equations of motion for granular drag in the regime relevant to our robot studies do not exist, we generated the vector fields in Fig. 4, D and E, by empirically estimating the forces acting on a robot limb moving through granular media in plate drag experiments (figs. S3, S5, and S6) [assuming the material was continuously deforming and thus in the “frictional fluid” regime (33, 35)]. Similar to previous studies (5, 33, 35), the measured force was a function of the drag angle between the limb tangent and velocity vectors (Fig. 4B, inset), depth of intrusion into the media, and media incline, and was insensitive to speed (within the relevant range).

In such non-inertial limb- and tail-driven locomotion, the interaction between the granular media and the limb is governed by the ratio of the perpendicular thrust forces to parallel drag forces. These ratios collapsed to a single curve across inclines, depths (Fig. 4B), and granular media (fig. S5 and supplementary materials). This collapse suggests that the change in performance on granular slopes in the crutching locomotion may be a consequence of the effect of gravity on the body. Because our drag measurements were made in freshly prepared media, and because we could not model the possible interactions with the footprints of previous steps (8), we confined our analysis to the first step, as with the robot. Further, only high adduction angles were considered, so that we could avoid the effects of an accumulating pile of granular media at the front of the robot

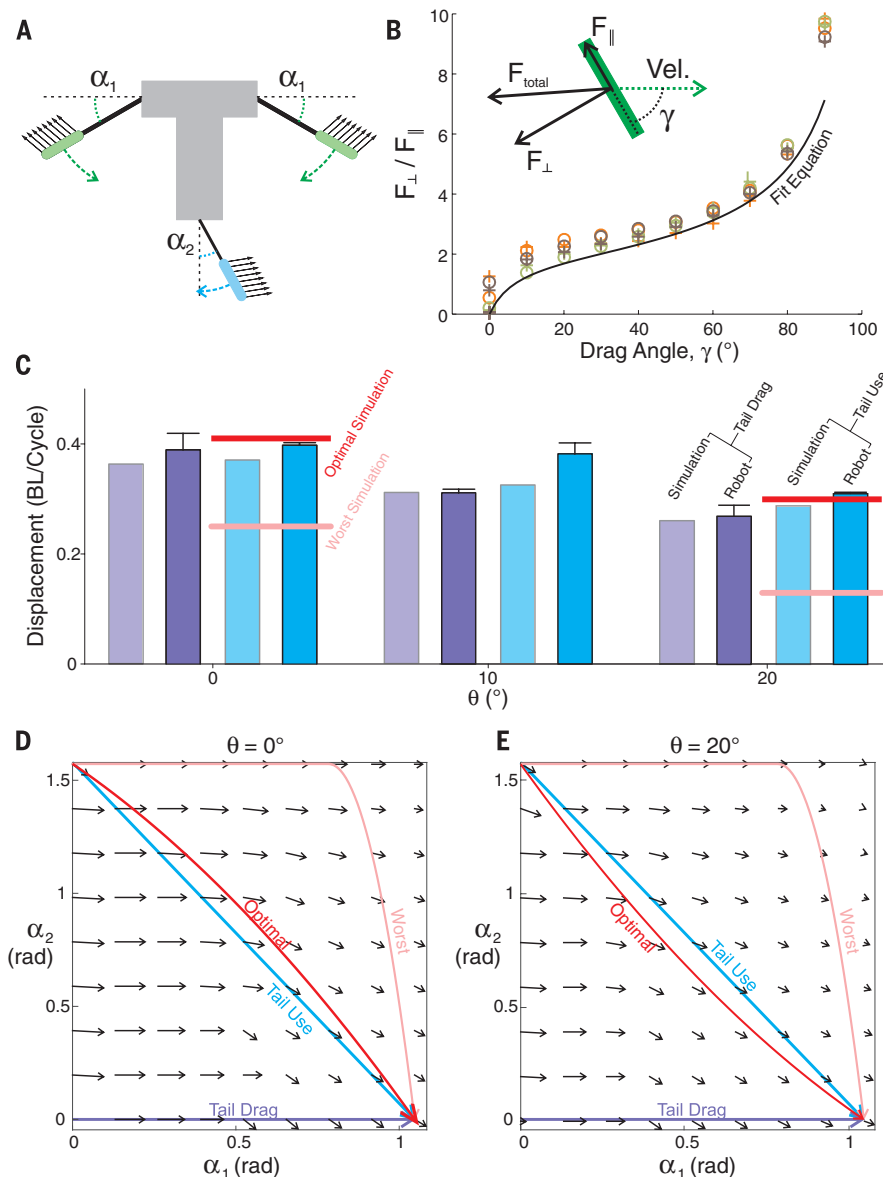


Fig. 4. Geometric mechanics model of MuddyBot locomotion. (A) A diagram of the simulation, showing the limb angle (α_1) and tail angle (α_2) as well as the reaction forces used to compute the local connection (see supplementary materials) between body deformation and body displacement. (B) The ratio of forces parallel and perpendicular to the limb surface during poppy seed drag experiments at various drag angles to the direction of motion, insertion depths, and substrate slopes. Intrusion depths are 1 cm (crosses) and 3 cm (circles), with $\theta = 0^\circ$ (brown), 20° uphill (orange), and 20° downhill (green). The black line represents the ratio of perpendicular and parallel equations (fitted independently; see supplementary materials). (C) First-step displacement (without slip) of the robot and simulation at all inclines ($\psi = 20^\circ$, $\phi = 0^\circ$), showing close agreement between the simulation and robot performance. Red and pink bars indicate the optimal and worst gaits, respectively. (D and E) Local connection vector field for $\theta = 0^\circ$ (D) and $\theta = 20^\circ$ (E) media, showing the limb only with tail dragging (purple) and tail gaits (light blue), as well as calculated optimal (red) and worst (pink) gaits.

when the body was insufficiently lifted. Additionally, when the tail was lifted clear of the media in robot experiments, the posterior motor and mounting structures intruded into and dragged through the media, resulting in an intrusion that was difficult to model; therefore, we simulated trials with the tail intruding into the media in the same configuration as at the end of tail-thrusting behavior, which yielded similar performance. To test these assumptions, we compared results to a subset of robot trials, and obtained good agreement between simulation and experiment (Fig. 4C and fig. S4).

The change in the patterns of the local connection vector fields revealed how limbs and tail could coordinate to produce movement (Fig. 4, C to E). For example, these fields demonstrated that the tail was not uniformly beneficial in all situations, nor even substantially beneficial in horizontal movement, in which the vertical component of the vectors (tail contribution) was small. However, as surface incline angle increased, the horizontal magnitudes of connection vectors decreased, indicating reduced efficacy of limb-only tail-dragging gaits (a horizontal path across the vector field). The relatively larger vertical component across more of the shape space indicated the increased importance of the tail to forward movement. The optimal gait for both inclines was close to the synchronous thrusting used by the robot and mudskipper, yielding similar displacements (Fig. 4, C to E); phase lag between initiation of limb and tail movement was suboptimal and, in one case per incline, yielded the worst possible gait (Fig. 4, D and E). Improper use of the tail resulted in substantially lower performance than simply allowing it to drag (Fig. 4, C to E). Additionally, the generally downward direction of the vectors in both fields demonstrate that purely tail-powered locomotion (a vertical path down the right of the vector field) can produce forward motion, as seen in some extant fish (12).

Our results from a biological analog of early tetrapods and robophysical and mathematical models demonstrate that the tail can play an important role in limb-driven crutching locomotion on inclined granular substrates by making locomotors more robust to suboptimal kinematics and substrate conditions. This suggests that the sizable, well-ossified (and presumably well-muscled) tails of early tetrapods (15–17), originally used for swimming, may have been co-opted to promote reliable locomotion over challenging substrates, providing an exaptation (36) that facilitated their invasion of land. Although evidence of tail use is absent among the few fossil trackways attributed to early tetrapods (37, 38), tail use might be evident in trackways formed on inclined shores.

REFERENCES AND NOTES

- J. A. Clack, *Gaining Ground: The Origin and Evolution of Tetrapods* (Indiana Univ. Press, 2002).
- E. B. Daeschler, N. H. Shubin, F. A. Jenkins Jr., *Nature* **440**, 757–763 (2006).
- A. Blicek et al., *Geol. Soc. London Spec. Publ.* **278**, 219–235 (2007).
- N. Gravish, P. B. Umbanhowar, D. I. Goldman, *Phys. Rev. Lett.* **105**, 128301 (2010).
- H. Marvi et al., *Science* **346**, 224–229 (2014).
- F. Qian et al., *Bioinspir. Biomim.* **10**, 056014 (2015).
- C. Li, P. B. Umbanhowar, H. Komsuoglu, D. E. Koditschek, D. I. Goldman, *Proc. Natl. Acad. Sci. U.S.A.* **106**, 3029–3034 (2009).
- N. Mazouchova, P. B. Umbanhowar, D. I. Goldman, *Bioinspir. Biomim.* **8**, 026007 (2013).
- J. Davenport, A. K. M. A. Matin, *J. Fish Biol.* **37**, 175–184 (1990).
- A. G. Johnels, *Oikos* **8**, 122 (1957).
- C. M. Pace, A. C. Gibb, *J. Exp. Biol.* **214**, 530–537 (2011).
- C. M. Pace, A. C. Gibb, *J. Fish Biol.* **84**, 639–660 (2014).
- A. Jusufi, D. I. Goldman, S. Revzen, R. J. Full, *Proc. Natl. Acad. Sci. U.S.A.* **105**, 4215–4219 (2008).
- T. Libby et al., *Nature* **481**, 181–184 (2012).
- E. Jarvik, *Medd. Gronl.* **114**, 1–90 (1952).
- E. Jarvik, *The Devonian Tetrapod Ichthyostega* (Indiana Univ. Press, 1996).
- M. I. Coates, *Trans. R. Soc. Edinb. Earth Sci.* **87**, 363–421 (1996).
- R. W. Blob, *Paleobiology* **27**, 14–38 (2001).
- M. A. Ashley-Ross, S. T. Hsieh, A. C. Gibb, R. W. Blob, *Integr. Comp. Biol.* **53**, 192–196 (2013).
- S. E. Pierce, J. A. Clack, J. R. Hutchinson, *Nature* **486**, 523–526 (2012).
- S. E. Pierce, J. R. Hutchinson, J. A. Clack, *Integr. Comp. Biol.* **53**, 209–223 (2013).
- E. M. Standen, T. Y. Du, H. C. E. Larsson, *Nature* **513**, 54–58 (2014).
- S. M. Kawano, R. W. Blob, *Integr. Comp. Biol.* **53**, 283–294 (2013).
- V. A. Harris, *Proc. Zool. Soc. London* **134**, 107–135 (1960).
- B. O. Swanson, A. C. Gibb, *J. Exp. Biol.* **207**, 4037–4044 (2004).
- J. Aguilera, D. I. Goldman, *Nat. Phys.* **12**, 278 (2016).
- A. Shapere, F. Wilczek, *Phys. Rev. Lett.* **58**, 2051–2054 (1987).
- R. L. Hatton, Y. Ding, H. Choset, D. I. Goldman, *Phys. Rev. Lett.* **110**, 078101 (2013).
- N. Mitarai, F. Nori, *Adv. Phys.* **55**, 1–45 (2006).
- S. S. Sharpe, R. Kuckuk, D. I. Goldman, *Phys. Biol.* **12**, 046009 (2015).
- H. Askari, K. Kamrin, <http://arxiv.org/abs/1510.02966> (2015).
- K. Nishikawa et al., *Integr. Comp. Biol.* **47**, 16–54 (2007).
- C. Li, T. Zhang, D. I. Goldman, *Science* **339**, 1408–1412 (2013).
- S. D. Kelly, R. M. Murray, *J. Robot. Syst.* **12**, 417–431 (1995).
- R. D. Maladen, Y. Ding, C. Li, D. I. Goldman, *Science* **325**, 314–318 (2009).
- S. J. Gould, E. S. Vrba, *Paleobiology* **8**, 4–15 (1982).
- J. Clack, *Palaeoogeogr. Palaeoclimatol. Palaeoecol.* **130**, 227–250 (1997).
- S. Curth, M. S. Fischer, J. A. Nyakatura, *Ichnos* **21**, 32–43 (2014).

ACKNOWLEDGMENTS

Supported by NSF grants PoLS PHY-1205878, PHY-1150760, and CMMI-1361778, Army Research Office (ARO) grant W911NF-11-0514, and the ARL MAST CTA (D.I.G.); ARO Robotics CTA and NSF National Robotics Initiative IIS-1426655 (H.C.); NSF grants IOS-0517340 and IOS-0817794 (R.W.B.); GT UROP and the GT PURA Travel Grant (B.M.); a Clemson University Wade Stackhouse Fellowship, NSF award DBI-1300426, and the University of Tennessee, Knoxville (S.M.K.); and the U.S. Department of Defense, Air Force Office of Scientific Research, National Defense Science and Engineering Graduate (NDSEG) Fellowship, 32 CFR 168a (P.E.S.). The authors declare no conflicts of interest. Data are available from the corresponding author upon request.

SUPPLEMENTARY MATERIALS

www.sciencemag.org/content/353/6295/154/suppl/DC1
Materials and Methods
Supplementary Text
Figs. S1 to S6
Table S1
Movies S1 to S6
References (39, 40)

16 December 2015; accepted 26 May 2016
10.1126/science.aaf0984

ROBOTICS

Phototactic guidance of a tissue-engineered soft-robotic ray

Sung-Jin Park,¹ Mattia Gazzola,^{2,*} Kyung Soo Park,^{3,4,†} Shirley Park,^{5,‡} Valentina Di Santo,⁶ Erin L. Blevins,^{6,§} Johan U. Lind,¹ Patrick H. Campbell,¹ Stephanie Dauth,¹ Andrew K. Capulli,¹ Francesco S. Pasqualini,¹ Seungkuk Ahn,¹ Alexander Cho,¹ Hongyan Yuan,^{1||} Ben M. Maoz,¹ Ragu Vijaykumar,⁵ Jeong-Woo Choi,^{3,4} Karl Deisseroth,^{5,7} George V. Lauder,⁶ L. Mahadevan,^{2,8} Kevin Kit Parker^{1,4,¶}

Inspired by the relatively simple morphological blueprint provided by batoid fish such as stingrays and skates, we created a biohybrid system that enables an artificial animal—a tissue-engineered ray—to swim and phototactically follow a light cue. By patterning dissociated rat cardiomyocytes on an elastomeric body enclosing a microfabricated gold skeleton, we replicated fish morphology at $1/_{10}$ scale and captured basic fin deflection patterns of batoid fish. Optogenetics allows for phototactic guidance, steering, and turning maneuvers. Optical stimulation induced sequential muscle activation via serpentine-patterned muscle circuits, leading to coordinated undulatory swimming. The speed and direction of the ray was controlled by modulating light frequency and by independently eliciting right and left fins, allowing the biohybrid machine to maneuver through an obstacle course.

Bioinspired design, as applied to robotics, aims at implementing naturally occurring features such as soft materials, morphologies, gaits, and control mechanisms in artificial settings in order to improve performance (1–4). For example, recent soft-robotics studies raised awareness on the importance of

material properties (3, 4), shifting the focus from rigid elements to soft materials, whereas other investigations report successful mimicry of gaits or morphological features inspired by insects (5, 6), fish (7, 8), snakes (9), salamanders (10), and cheetahs (11). Although recent advances have the promise of bridging the performance gap with animals,

Tail use improves performance on soft substrates in models of early vertebrate land locomotors

Benjamin McInroe, Henry C. Astley, Chaohui Gong, Sandy M. Kawano, Perrin E. Schiebel, Jennifer M. Rieser, Howie Choset, Richard W. Blob and Daniel I. Goldman

Science **353** (6295), 154-158.
DOI: 10.1126/science.aaf0984

ARTICLE TOOLS

<http://science.sciencemag.org/content/353/6295/154>

SUPPLEMENTARY MATERIALS

<http://science.sciencemag.org/content/suppl/2016/07/07/353.6295.154.DC1>

RELATED CONTENT

<http://science.sciencemag.org/content/sci/353/6295/120.full>

REFERENCES

This article cites 36 articles, 10 of which you can access for free
<http://science.sciencemag.org/content/353/6295/154#BIBL>

PERMISSIONS

<http://www.sciencemag.org/help/reprints-and-permissions>

Use of this article is subject to the [Terms of Service](#)

Science (print ISSN 0036-8075; online ISSN 1095-9203) is published by the American Association for the Advancement of Science, 1200 New York Avenue NW, Washington, DC 20005. The title *Science* is a registered trademark of AAAS.

Copyright © 2016, American Association for the Advancement of Science